Supplemental information for

Kinetics of the nitrate-mediated photooxidation of monocarboxylic acids in the aqueous phase

Yuting Lyu,[a,b] Jany Ting Chun Chow,[a] Theodora Nah[a,b*]

[a]*School of Energy and Environment, City University of Hong Kong, Hong Kong SAR, China*
[b]*State Key Laboratory of Marine Pollution, City University of Hong Kong, Hong Kong SAR, China*

* To whom correspondence should be addressed: Theodora Nah (Email: theodora.nah@cityu.edu.hk, Tel: +852 3442 5578, Postal address: School of Energy and Environment, Yeung Kin Man Academic Building, City University of Hong Kong, Tat Chee Avenue, Kowloon, Hong Kong)
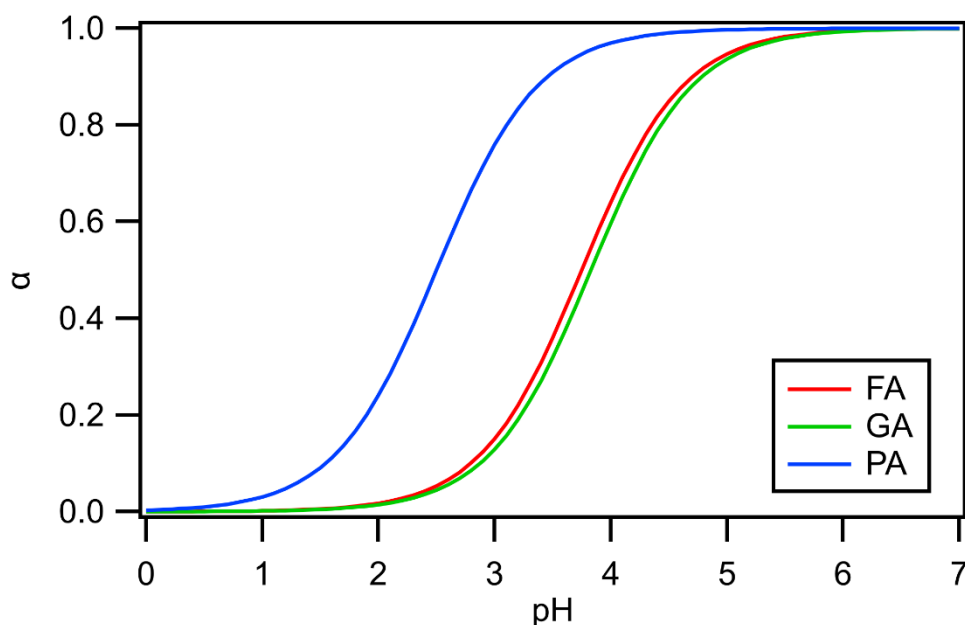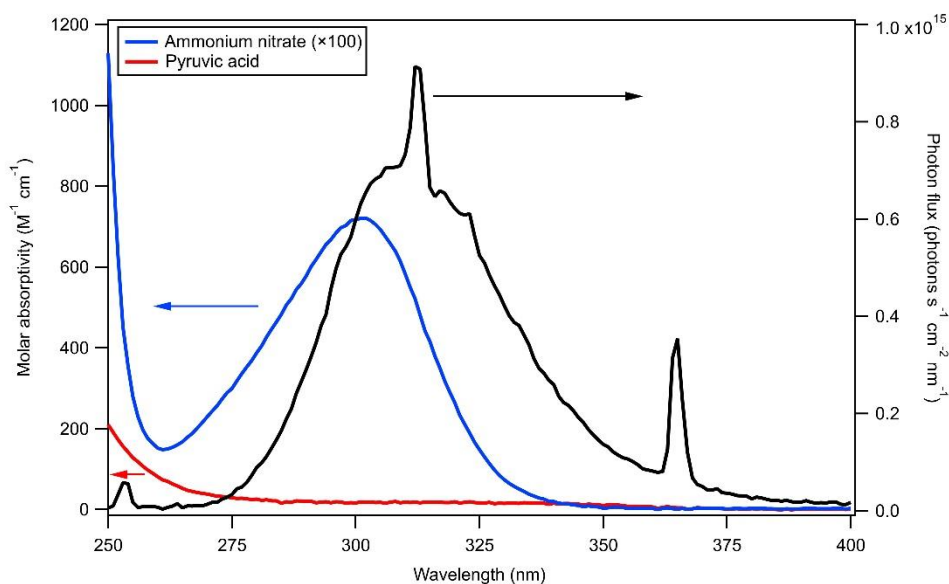
35

36 **Figure S1.** Dissociation curves of FA, GA, and PA. The pK_a values used for the calculation of

37 FA, GA, and PA were 3.75[1], 3.82[2], and 2.50[3], respectively.

38

39 **Figure S2.** The photon flux in the photoreactor and the molar absorptivity ammonium nitrate

40 and pyruvic acid. Note that the molar absorptivity values of ammonium nitrate shown here

41 have been multiplied by 100 for easier comparison. The molar absorptivities of ammonium

42 nitrate and pyruvic acid were obtained using 104 mM and 1 mM solutions, respectively, since

43 the absorption signals for 250/1250 µM ammonium nitrate and 10 µM pyruvic acid were very

44 low. The photon flux in the photoreactor was determined using the method detailed by Li et al.

45 (2022).[4]
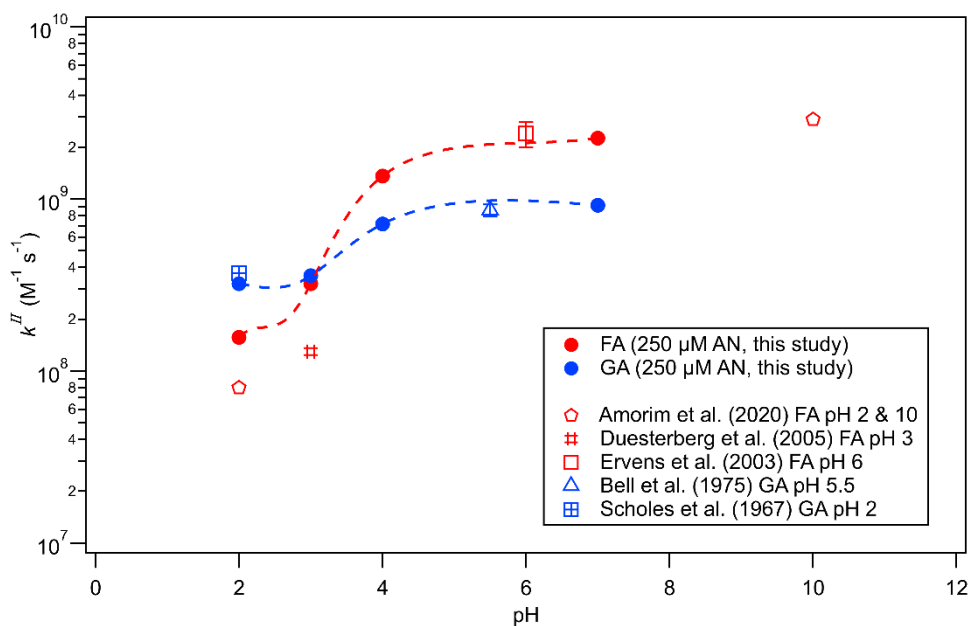
Figure S3. Calculated second-order rate constants (k^{II}) vs. pH using actual k_{obs} and estimated [OH]$_{ss}$ values from this study (filled blue and red symbols). Dotted lines are used to guide the eyes. We assumed that k_{obs} was the product of k^{II} and [·OH]$_{ss}$. Also included are the k^{II} values for FA and GA from previous studies.[1, 5-8] Note that the y axis is presented in a logarithm scale to accommodate the drastically different k^{II} of FA at pH 2 and pH 10 reported by Amorim et al. (2020) and Ervens et al. (2003).
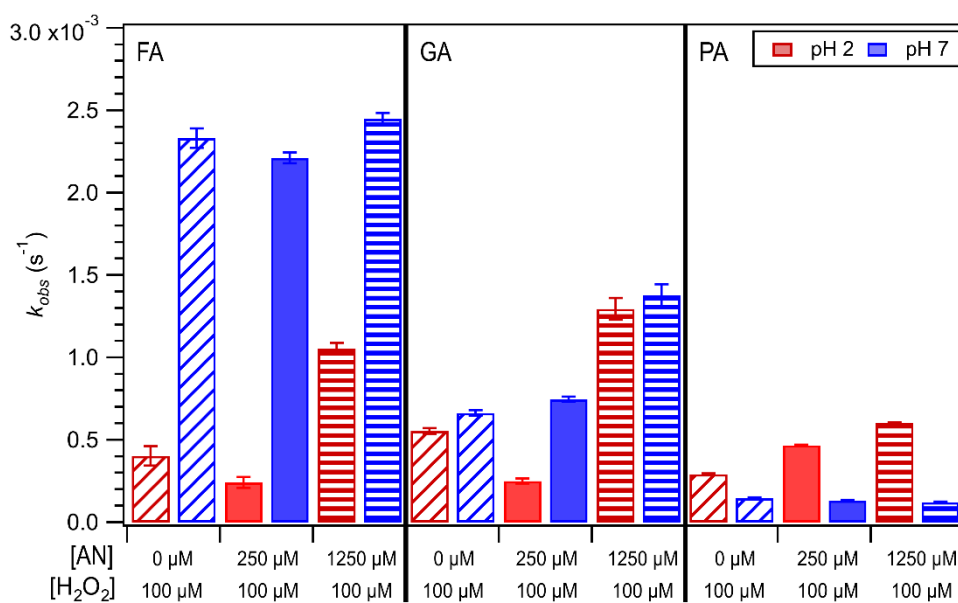
Figure S4. k_{obs} of FA, GA, and PA at pH 2 and 7. The carboxylic acid concentrations were fixed at 10 μM, the H$_2$O$_2$ concentration was fixed at 100 μM, while either 0 μM or 250 μM or 1250 μM AN were used in these experiments. Error bars indicate standard deviation of multiple experiments.
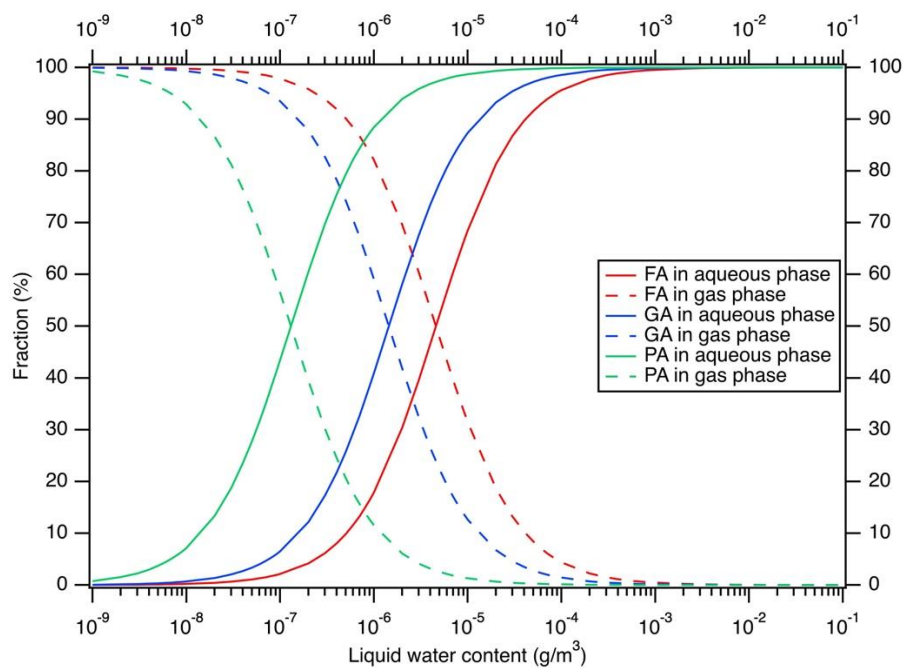
58

59 **Figure S5.** Calculated carboxylic acids partitioning between gas phase and aqueous phase as a

60 function of liquid water content (LWC). The Henry's law solubility coefficients used for

61 calculation are listed in Table S5.

62

63

64

65

66

67

68

69

70

71

72

73 **Table S1.** Concentrations of NH$_4$OH or H$_2$SO$_4$ in the solutions and the resulting ionic strengths

74 (I) of the solutions.

Solution pH	NH$_4$NO$_3$	NH$_4$OH	H$_2$SO$_4$	I
2	250 μM	0	0.00535 M	0.01095 M
2	1250 μM	0	0.00535 M	0.01195 M
3	250 μM	0	0.00107 M	0.00239 M
3	1250 μM	0	0.00107 M	0.00309 M
4	250 μM	0	0	0.00025 M
4	1250 μM	0	0	0.00125 M
7	250 μM	0.000039 M	0	0.0002695 M
7	1250 μM	0.000039 M	0	0.0012695 M

75

76 **Table S2.** List of reactions pathways initiated by the aqueous photolysis of inorganic nitrate. [9-

77 13]

No.	Reactions	Quantum yield (Φ)/ Acid dissociation constant (pK$_a$)
1	NO$_3^-$ + hν → [•NO$_2$ + O•$^-$]$_{cage}$	Φ = 0.01
2	[•NO$_2$ + O•$^-$]$_{cage}$ → •NO$_2$ + O•$^-$	—
3	O•$^-$ + H$_2$O ⇆ •OH + OH$^-$	pK$_a$(•OH) = 11.9
4	[•NO$_2$ + O•$^-$]$_{cage}$ → OONO$^-$	—
5	OONO$^-$ + H$^+$ ⇆ HOONO	pK$_a$ = 7
6	HOONO → •OH + •NO$_2$	—
7	2 •NO$_2$ ⇆ N$_2$O$_4$	—
8	N$_2$O$_4$ + H$_2$O → HNO$_2$ + NO$_3^-$ + H$^+$	—
9	HNO$_2$ ⇆ H$^+$ + NO$_2^-$	pK$_a$ = 3 ~ 3.5
10	NO$_2^-$ + hν → •NO + O•$^-$	Φ = 0.025–0.065
11	NO$_2^-$ + hν → •NO$_2$ + e$^-$	Φ = ~ 0.001
12	NO$_2^-$ + •OH → •NO$_2$ + OH$^-$	—
13	•NO + •NO$_2$ ⇆ N$_2$O$_3$	—
14	N$_2$O$_3$ + H$_2$O → 2 NO$_2^-$ + 2 H$^+$	—

15	$HNO_2 + h\nu \rightarrow \bullet NO + \bullet OH$	$\Phi = 0.35$
16	$HNO_2 + \bullet OH \rightarrow \bullet NO_2 + H_2O$	—
17	$2\ HNO_2 \rightarrow \bullet NO + \bullet NO_2 + H_2O$	—

Table S3. Dissociation fractions for FA and GA used to calculate k_{OH}.

	FA		GA	
	HA	A^-	HA	A^-
pH 2	98.3%	1.7%	98.5%	1.5%
pH 3	84.9%	15.1%	87.1%	12.9%
pH 4	18.3%	81.7%	21.2%	78.8%
pH 7	0.01%	99.9%	0.01%	99.9%

Table S4. Second-order rate constants (k_{rxn}^{HA+OH} and $k_{rxn}^{A^-+OH}$) for the HA and A^- forms of FA and GA

FA				GA			
HA ($M^{-1}\ s^{-1}$)	Ref.	A^- ($M^{-1}\ s^{-1}$)	Ref.	HA ($M^{-1}\ s^{-1}$)	Ref.	A^- ($M^{-1}\ s^{-1}$)	Ref.
1.0×10^8	1	2.4×10^9	1	3.8×10^8	7	$(8.6 \pm 0.7) \times 10^8$	6
0.8×10^8	5	2.9×10^9	5				

Note: The average of two rate constants were used to calculate the simulated k_{obs} of FA.

Table S5. Parameters used to calculate the first-order rate constants of FA, GA, and PA in Figure 7.

		FA	Ref.	GA	Ref.	PA	Ref.
Property	pK_a	3.75	1	3.82	2	2.5	3
	K_H	88 mol cm^{-3} Pa^{-1}	14	280 mol cm^{-3} Pa^{-1}	14	3100 mol cm^{-3} Pa^{-1}	14
Gas	$k_{rxn,g}^{\cdot OH}$	6.24×10^{-7} cm^3 molec.$^{-1}$ s^{-1}	15	3.11×10^{-6} cm^3 molec.$^{-1}$ s^{-1}	16	*4.60×10^{-4} s^{-1}	17
Aerosols (pH 3)	$k_{rxn,aq}^{\cdot OH}$	3.22×10^8 M^{-1} s^{-1}	This study	3.58×10^8 M^{-1} s^{-1}	This study	*1.91×10^{-4} s^{-1}	This study
Clouds (pH 4)	$k_{rxn,aq}^{\cdot OH}$	1.36×10^9 M^{-1} s^{-1}	This study	7.16×10^8 M^{-1} s^{-1}	This study	*7.73×10^{-5} s^{-1}	This study

* Direct photolysis rates were used instead of much slower rate constants with $\cdot OH$.

Section S1. SPE protocol and UPLC-MS measurements of BA and PHBA

SPE was performed to desalt the samples using SPE cartridges (Oasis MAX, 60 mg, 3 cc, 60 µm, Waters). First, the sorbent was conditioned and equilibrated using 3 mL methanol (LC-MS grade) followed by 3 mL Milli-Q water. Next, the cartridge was loaded with 3 mL of 1× diluted sample solutions and then purged with 6 mL Milli-Q water. A vacuum pump was used to dry out the sorbent before elution using 3 mL 2% formic acid (LC-MS grade) in methanol (LC-MS grade). All the desalted samples were filtered using 0.2 µm nylon syringe membrane to remove any particulates prior to UPLC-MS analysis.

UPLC-MS analyses were performed using a reverse phase Kinetex Polar C18 column (2.6 µm, 150 × 2.1 mm) equipped with a Polar C18 guard column. For the mobile phase, eluent A was 10 mM ammonia acetate (LC-MS grade) in Milli-Q water buffered with 0.03% acetic acid (LC-MS grade), and eluent B was pure methanol (LC-MS grade). A gradient elution program was used, and it was delivered at a flow rate of 0.3 mL min^{-1}. The following mobile phase gradient was used for the detection of BA and its product PHBA: 0 to 3 min 1% B, 3 to 5 min linear rise to 80% B and hold to 6 min, 6 to 6.5 min linear drop to 1 % B and then hold to 10 min for equilibrium. The sample injection volume was set to 10 µL. The following tandem MS conditions were used: -4500 V ESI ion spray voltage, 80 V declustering potential, -20 V collision energy, 50 psi ion source gas, 25 psi curtain gas, and 450 ℃ source temperature.

Section S2. Calculations of the first-order rate constants of FA, GA, and PA

We used a similar methodology as the one used by Yang et al. (2021) to calculate the first-order rate constants of FA, GA, and PA.[18] Briefly, to represent the realistic conditions of atmospheric aqueous phase, we used the liquid water content (LWC) and pH of aqueous aerosols and clouds compiled by Herrmann et al. (2015).[19] We used pH 3 and 4 as the pH conditions of aqueous aerosols and cloud water, respectively, which are close to their global average pH values reported by previous studies.[20, 21] The LWC values used for the first-order decays of carboxylic acids in aerosols and clouds were set to 3×10^{-5} g m^{-3} and 1 g m^{-3}, respectively. The fraction of the three carboxylic acids present in the gas and aqueous phases as a function of LWC is shown in Figure S5. The fractions were calculated using the Henry's law solubility coefficient, K_H, and the method described by Witkowski et al. (2019).[22] The concentrations of ·OH ([·OH]) in the gas phase, aerosols, and clouds were set to 1×10^{6} molecules cm^{-3}, 5×10^{-13} M, and 5×10^{-14} M, respectively. The first-order rate constants of FA

118 and GA in the gas phase (k_g^I, s^{-1}) and aqueous aerosols/clouds ($k_{aerosols/clouds}^I$, s^{-1}) were

119 subsequently calculated using following equations:

120 $$k_g^I = \frac{k_{Heff} \times LWC}{1 + k_{Heff} \times LWC} \times k_{rxn,g}^{OH\cdot} \times [\cdot OH]_{gas} \qquad (S1)$$

121 $$k_{aerosols/clouds}^I = \frac{1}{1 + k_{Heff} \times LWC} \times k_{rxn,g}^{OH\cdot} \times [\cdot OH]_{aq} \qquad (S2)$$

122 where k_{Heff} is the effective Henry's law constants and is expressed as:

123 $$k_{Heff} = k_H \times (1 + \frac{[H^+]}{K_a}) \qquad (S3)$$

124 It should be noted that photolysis is the dominant sink of PA in both the atmospheric gas phase

125 and aqueous phase. The PA photolysis rate is nearly two orders of magnitude faster than the

126 rate of its reaction with $\cdot$OH.[17, 23] Therefore, we used the direct photolysis rates from the

127 literature (gas phase) and from this study (aqueous phase) to simulate the decay and lifetime of

128 PA in atmosphere. The parameters used to calculate the first-order rate constants of FA, GA,

129 and PA are summarized in Table S5.

130

131 **References**

132 1.   B. Ervens, S. Gligorovski and H. Herrmann, Temperature-dependent rate constants
133   for hydroxyl radical reactions with organic compounds in aqueous solutions, *Physical*
134   *Chemistry Chemical Physics*, 2003, **5**, 1811-1824.
135 2.   A. Williams, pKa Data Compiled by R. Williams.
136 3.   C. J. Clarke, J. A. Gibbard, L. Hutton, J. R. R. Verlet and B. F. E. Curchod,
137   Photochemistry of the pyruvate anion produces CO2, CO, CH3-, CH3, and a low
138   energy electron, *Nat Commun*, 2022, **13**.
139 4.   Y. Li, Y. He, C. H. Lam and T. Nah, Environmental photochemistry of organic UV
140   filter butyl methoxydibenzoylmethane: Implications for photochemical fate in surface
141   waters, *Science of The Total Environment*, 2022, **839**, 156145.
142 5.   J. V. Amorim, S. Wu, K. Klimchuk, C. Lau, F. J. Williams, Y. Huang and R. Zhao,
143   pH Dependence of the OH Reactivity of Organic Acids in the Aqueous Phase,
144   *Environ Sci Technol*, 2020, DOI: 10.1021/acs.est.0c03331.
145 6.   J. A. Bell, E. Grunwald and E. Hayon, Kinetics of deprotonation of organic free
146   radicals in water. Reaction of glycolate (HOCHCO2-), (HOCHCONH2), and
147   (HOCCH3CONH2) with various bases, *Journal of the American Chemical Society*,
148   1975, **97**, 2995-3000.
149 7.   G. Scholes and R. L. Willson, γ-Radiolysis of aqueous thymine solutions.
150   Determination of relative reaction rates of OH radicals, *Transactions of the Faraday*
151   *Society*, 1967, **63**, 2983-2993.
152 8.   C. K. Duesterberg, W. J. Cooper and T. D. Waite, Fenton-mediated oxidation in the
153   presence and absence of oxygen, *Environ Sci Technol*, 2005, **39**, 5052-5058.
154 9.   J. Mack and J. R. Bolton, Photochemistry of nitrite and nitrate in aqueous solution: a
155   review, *J Photoch Photobio A*, 1999, **128**, 1-13.

156 10. N. K. Scharko, A. E. Berke and J. D. Raff, Release of nitrous acid and nitrogen
157   dioxide from nitrate photolysis in acidic aqueous solutions, *Environ Sci Technol*,
158   2014, **48**, 11991-12001.
159 11. S. Gligorovski, R. Strekowski, S. Barbati and D. Vione, Environmental Implications
160   of Hydroxyl Radicals (center dot OH), *Chemical Reviews*, 2015, **115**, 13051-13092.
161 12. H. Herrmann, On the photolysis of simple anions and neutral molecules as sources of
162   O−/OH, SOx− and Cl in aqueous solution, *Physical Chemistry Chemical Physics*,
163   2007, **9**, 3935-3964.
164 13. G. Marussi and D. Vione, Secondary Formation of Aromatic Nitroderivatives of
165   Environmental Concern: Photonitration Processes Triggered by the Photolysis of
166   Nitrate and Nitrite Ions in Aqueous Solution, *Molecules*, 2021, **26**, 2550.
167 14. R. Sander, Compilation of Henry's law constants (version 4.0) for water as solvent,
168   *Atmospheric Chemistry and Physics*, 2015, **15**, 4399-4981.
169 15. J. M. Anglada, Complex Mechanism of the Gas Phase Reaction between Formic Acid
170   and Hydroxyl Radical. Proton Coupled Electron Transfer versus Radical Hydrogen
171   Abstraction Mechanisms, *Journal of the American Chemical Society*, 2004, **126**,
172   9809-9820.
173 16. W. M. Meylan and P. H. Howard, Computer estimation of the Atmospheric gas-phase
174   reaction rate of organic compounds with hydroxyl radicals and ozone, *Chemosphere*,
175   1993, **26**, 2293-2299.
176 17. A. E. Reed Harris, J.-F. Doussin, B. K. Carpenter and V. Vaida, Gas-Phase Photolysis
177   of Pyruvic Acid: The Effect of Pressure on Reaction Rates and Products, *The Journal*
178   *of Physical Chemistry A*, 2016, **120**, 10123-10133.
179 18. X. Yang, Y. Tao and J. G. Murphy, Kinetics of the oxidation of ammonia and amines
180   with hydroxyl radicals in the aqueous phase, *Environmental Science: Processes &*
181   *Impacts*, 2021, **23**, 1906-1913.
182 19. H. Herrmann, Kinetics of Aqueous Phase Reactions Relevant for Atmospheric
183   Chemistry, *Chemical Reviews*, 2003, **103**, 4691-4716.
184 20. H. O. T. Pye, A. Nenes, B. Alexander, A. P. Ault, M. C. Barth, S. L. Clegg, J. L.
185   Collett, Jr., K. M. Fahey, C. J. Hennigan, H. Herrmann, M. Kanakidou, J. T. Kelly, I.
186   T. Ku, V. F. McNeill, N. Riemer, T. Schaefer, G. Shi, A. Tilgner, J. T. Walker, T.
187   Wang, R. Weber, J. Xing, R. A. Zaveri and A. Zuend, The Acidity of Atmospheric
188   Particles and Clouds, *Atmos Chem Phys*, 2020, **20**, 4809-4888.
189 21. V. Shah, D. J. Jacob, J. M. Moch, X. Wang and S. Zhai, Global modeling of cloud
190   water acidity, precipitation acidity, and acid inputs to ecosystems, *Atmos. Chem.*
191   *Phys.*, 2020, **20**, 12223-12245.
192 22. B. Witkowski, M. Al-sharafi and T. Gierczak, Ozonolysis of β-Caryophyllonic and
193   Limononic Acids in the Aqueous Phase: Kinetics, Product Yield, and Mechanism,
194   *Environmental Science & Technology*, 2019, **53**, 8823-8832.
195 23. A. E. Reed Harris, B. Ervens, R. K. Shoemaker, J. A. Kroll, R. J. Rapf, E. C. Griffith,
196   A. Monod and V. Vaida, Photochemical Kinetics of Pyruvic Acid in Aqueous
197   Solution, *The Journal of Physical Chemistry A*, 2014, **118**, 8505-8516.
198